Colloids and Surfaces B: Biointerfaces 157 (2017) 391–397

Contents lists available at ScienceDirect

Colloids and Surfaces B: Biointerfaces

journal homepage: www.elsevier.com/locate/colsurfb

Protocols

Optimizing purification process of MIM-I-BAR domain by introducing atomic force microscope and dynamics simulations

Yue Zhang[a,b], Zhichao Lou[a,c], Xubo Lin[d], Qiwei Wang[a,b], Meng Cao[b], Ning Gu[a,b,*]

[a] State Key Laboratory of Bioelectronics, Jiangsu Key Laboratory for Biomaterials and Devices, School of Biological Science & Medical Engineering, Southeast University, Nanjing, 210096, China
[b] Collaborative Innovation Center of Suzhou Nano Science and Technology, Suzhou 215123, China
[c] College of Materials Science and Engineering, Nanjing Forestry University, Nanjing 210037, China
[d] Department of Integrative Biology and Pharmacology, McGovern Medical School, The University of Texas Health Science Center at Houston, Houston, TX 77030, United States

ARTICLE INFO

Article history:
Received 30 March 2017
Received in revised form 10 May 2017
Accepted 20 May 2017
Available online 26 May 2017

Keywords:
Atomic force microscopy
Dynamics simulations
I-BAR domain
Purification optimization
Recombinant expression

ABSTRACT

MIM (missing in metastasis) is a member of I-BAR (inverse BAR) domain protein family, which functions as a putative metastasis suppressor. However, methods of gaining high purity MIM-I-BAR protein are barely reported. Here, by optimizing the purification process including changing the conditions of cell lysate and protein elution, we successfully purified MIM protein. The purity of the obtained protein was up to ~90%. High-resolution atomic force microscope (AFM) provides more visual images, ensuring that we can observe the microenvironment around the target protein, as well as the conformations of the purification products following each purification process. MIM protein with two different sizes were observed on mica surface with AFM. Combining with molecular dynamics simulations, these molecules were revealed as MIM monomer and dimer. Furthermore, our study attaches importance to the usage of imidazole with suitable concentrations during the affinity chromatography process, as well as the removal of excessive imidazole after the affinity chromatography process. All these results indicate that the method described here was successful in purifying MIM protein and maintaining their natural properties, and is supposed to be used to purify other proteins with low solubility.

1. Introduction

Owing to the important roles in the regulation of membrane changes, certain membrane-associated proteins such as BAR family proteins, have drawn increasing interests in the medical fields [1]. Among them, metastasis suppressor 1 (MIM) is a special protein with abnormal expression in tumor tissues [2]. Previous publications confirmed that MIM is overexpressed in primary tumors but lost in metastatic cancer cells [4]. MIM protein represents the typical characteristics of I-BAR proteins, which are mainly related to the direct/indirect regulation for cytoskeleton [5]. BAR domain of MIM protein, consisting of 250 amino acids, is critical for MIM function and binds to phosphatidylinositol (4, 5)-bisphosphate (PIP2) enriched membranes [6]. Recombinant MIM-I-BAR is proved to be useful in many fields [7], so far methods of gaining high purity MIM-I-BAR protein are barely reported yet.

In this work, we aimed to express MIM-I-BAR with more natural properties in bacteria, avoiding unwanted denaturation and refolding process. The solubility of MIM-I-BAR was improved by changing the lysate conditions. Ni-NTA resin chromatography and desalination/ultrafiltration step were necessary in this work to purify the soluble protein. The application of AFM in characterizing the molecular size and morphology of protein has gradually become research hotspot [8].

Compared with traditional investigation technologies, such as X-ray diffraction and nuclear magnetic resonance, AFM provides additional information on 3D morphology of biomolecules, and ensures the researchers to investigate the conformation evolutions of the target molecules during the bioengineering processes. Here, we introduce high-resolution AFM imaging technology to in-depth investigate the conformations of the products from each process of the purification. Combining the results of AFM and the molecular

* Corresponding author at: State Key Laboratory of Bioelectronics, Jiangsu Key Laboratory for Biomaterials and Devices, School of Biological Science & Medical Engineering, Southeast University, Nanjing, 210096, China.
E-mail address: guning@seu.edu.cn (N. Gu).

http://dx.doi.org/10.1016/j.colsurfb.2017.05.054
0927-7765/

dynamics simulations, we confirmed that we successfully obtained MIM-I-BAR with high purity, and they present in the solution in the forms of monomer and dimer. Besides, our study attaches importance to the usage of imidazole with suitable concentrations during the affinity chromatography process, as well as the removal of excessive imidazole after the affinity chromatography process. All these results indicate that the method described here was successful in purifying MIM protein and maintaining their natural properties, and is supposed to be used to purify other proteins with low solubility.

2. Materials and methods

2.1. Bacterial strain and materials

Ni-NTA resin was purchased from Genscript (China). *E. coli* BL21 (DE3) strain and DNA agarose were purchased from Invitrogen (USA). Sodium dodecyl sulfate polyacrylamide gel electrophoresis (SDS-PAGE) gel preparation kit was purchased from Beyotime (China). All the other chemicals needed in this work were purchased from Sigma Aldrich (USA).

2.2. In vitro *expression of MIM-I-BAR*

Plasmids encoding His tagged MIM-I-BAR proteins were prepared by ligation of PCR-generated DNA fragments into vectors pET-14b (Novagen). DNA cloning was performed in DH5α cells. The primers used in PCR were listed in Table 1.

Briefly, chemically competent BL21 (DE3) *E. coli* cells were transformed with pET14b-MIM-I-BAR. The transformed cells were selected based on their resistance to ampicillin. A single colony of the transformed cells incubated in 3 mL of Lennox broth medium (LB, 1% tryptone, 0.5% yeast extract, 1% NaCl, 50 μg ampicillin mL^{-1}, pH 7.4) at 37° C for 8 h at shaking speed of 220 revolutions per minute. The culture was further inoculated in 150 mL of pre-warmed LB medium and shaked at 37° C, 220 revolutions per minute for another 2 h. When the optical density at 600 nm reached to 0.6, the culture was added with 0.4 mmol isopropyl-beta-D-thiogalactopyranoside (IPTG) L^{-1}, and cells were collected by centrifugation (5752*g*, 15 min, 4 °C) 3 h later. The cell pellets were stored at −20 °C.

2.3. Purification of MIM-I-BAR

A cell pellet mentioned above was re-suspended in 5 mL lysate buffer consisting of 50 mmol Tris/HCl L^{-1}, 500 mmol NaCl L^{-1}, 10 mmol Imidazole L^{-1}, 1 mmol PMSF L^{-1}, and 0.2 mg lysozyme mL^{-1}. 1 uL protease inhibitor cocktail mL^{-1} (KeyGEN, China) was added. Then the mixture was kept at −80 °C overnight. After that, the re-suspended cells were sonicated on ice for 5 min (work for 2 s, interval for 3 s). The soluble fraction was collected by centrifugation (15000 revolutions per minute, 40 min, 4 °C) and loaded onto a pre-packed 2 mL Ni-NTA agarose column, which was previously equilibrated with ten column volumes of Buffer A containing 20 mmol phosphate buffer L^{-1}, 500 mmol NaCl L^{-1} and 10 mmol Imidazole L^{-1}. The purity of protein was improved by gradient elution. The optimum concentration of imidazole for each experiment was tested firstly. The eluted protein was desalted using a PD-10 column (GE, USA) and condensed by ultrafiltration (5000 revolutions per minute, 20 min, 4 °C). The obtained products was stored in PBS (pH7.4) in −80 °C. The purity of the product was determined by 10% SDS-PAGE.

2.4. Atomic force microscope imaging

AFM was introduced to investigate the conformations of the obtained products after each step in our purification process. AFM imaging was carried out with utilizing an Agilent 5500 AFM system (Agilent, Chandler, AZ). The sample solution was diluted in PBS and dropped on freshly cleaved mica surface. After 5 min incubation, the surface was washed with PBS for 4-5 times and dried in the air. Silicon cantilevers tip with spring constant of around 0.1 N/m was used for imaging. The AFM imaging was performed in air at room temperature in Agilent AAC mode. The obtained AFM images were processed by WSxM software [9].

2.5. Molecular dynamics simulations

Martini coarse-grained (CG) force field (version 2.1) [10] were used for modelling the dynamics of MIM I-BAR in the mixture of imidazole and water with the molar ratio 1:1. CG parameter of MIM I-BAR was obtained by using the tool *seq2itp.pl*, which used the information of amino acid sequence (Fig. 2A) and secondary structure (PDB ID: 2D1L). As for imidazole, known ring fragment in Martini model was used to get the its CG model. The detailed parameters could be found in supporting information (*.itp files). In order to study whether MIM I-BAR preferred to interact with imidazole, we set up the initial simulation system with MIM I-BAR centered in the box (dimension: 21nm × 21nm × 21 nm), and further evenly solvated the box with 28577 imidazole and 28577 water molecules. (Fig. 1)

The system was firstly kept at T = 400 K for 10 ns to mimic the initial randomly distributed states, and then the temperature was gradually lowered down to room temperature (T = 298 K). All the simulations were performed for 2.4 μs (effective time) with a time step of 20 fs and periodic boundary conditions using GROMACS 5.0.4 [11]. The first 400 ns simulation was reserved for system equilibrium. Snapshots of the simulation system in this paper were all rendered by VMD [12]. For all simulations, a cutoff of 1.2 nm was used for van der Waals (vdW) interactions, and the Lenard-Jones potential was smoothly shifted to zero between 0.9 nm and 1.2 nm to reduce cutoff noise. For electrostatic interactions, the columbic potential, with a cutoff of 1.2 nm, was smoothly shifted to zero from 0 to 1.2 nm. The relative dielectric constant was 15, which was the default value of the force field [13]. MIM I-BAR, imidazole and water were coupled separately to V-rescale heat baths [14] at T = 298 K, with a coupling constant τ=1 ps. The systems were simulated at 1 bar pressure using isotropic Parrinello-Rahman pressure coupling scheme [15] with a coupling constant τ = 5 ps and the compressibility of 3×10^{-4}. The neighbor list for non-bonded interactions was updated every 10 steps with the cut-off 1.4 nm.

3. Results and discussion

3.1. Recombinant plasmid construction and in vitro protein expression

The vector plasmid pET-14b contains 6 × His-tag at the N-terminal of the cloned gene, which could be easily expressed in the *E. coli* BL21 (DE3) prokaryotic expression system and purified using nickel ion beads (Cao M et al., 2014).The MIM-I-BAR sequence comprising amino acid residues (aa) 1–235 is shown in Fig. 2A. The plasmid construct map is shown in Fig. 2B. MIM conformation predicted by dynamics simulation is shown in Fig. 2C.

Following IPTG induction, soluble MIM-I-BAR was present in the supernatant of the cell lysate and the supernatant was analyzed by Western blot using the anti-histidine antibody and anti-MIM antibody. Fig. 3 showed western blot results of the products with-

Table 1
Designed primers for PCR.

Gene name	Designed primers	
His-MIM-I-BAR	Sense	5′-CAGTTACTCGAGGAGGCTGTGATCGAGAAGG-3′
	Anti-sense	5′-GTCGGATCCTTAGTCCAAAATCACCTGTTCAC-3′

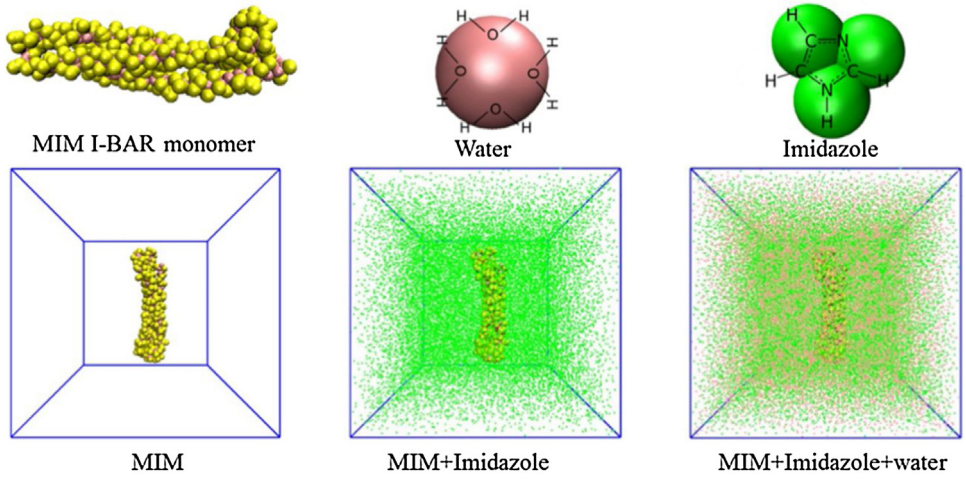

Fig. 1. Simulation system, coloring style is the same as above. The system consists of 1 MIM I-BAR monomer, 28577 Imidazole and 28577 water.

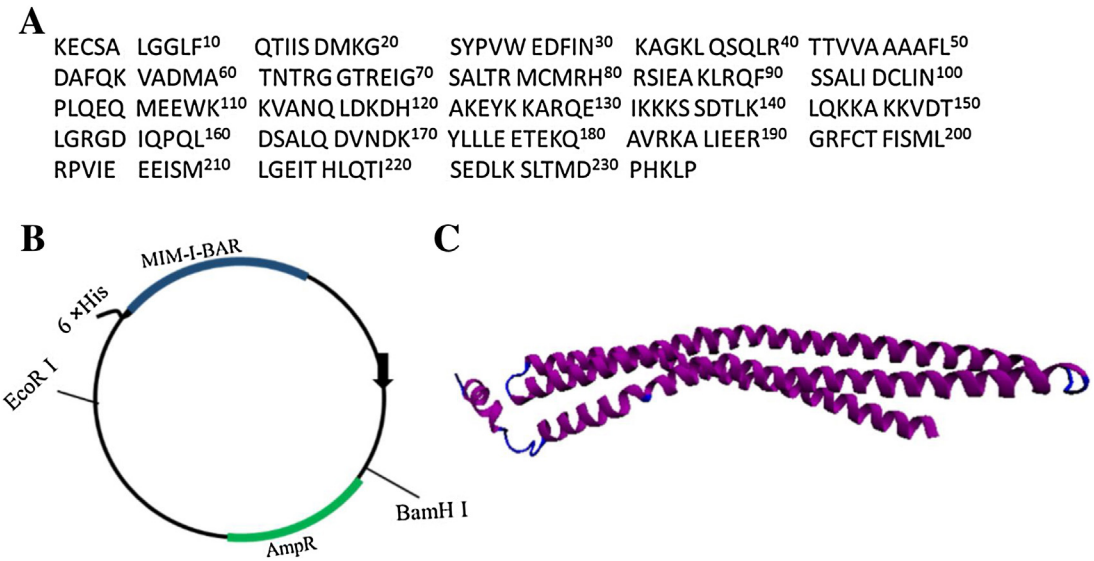

Fig. 2. (A) The amino acid sequences of MIM-I-BAR, I-BAR, reverse Bin-Amphiphysin-Rvs. (B) Plasmid Construct Map. 6 × His,His tag; MIM-I-BAR, MIM protein domain; AmpR, Remove the AMP(antibiotic) toxicity; EcoR I and BamH I, cleavage sites (C) Overall conformation of MIM I-BAR with the structure adapted from Protein Data Bank (ID: 2D1L) [16]. The alpha-helix is in purple, while the other second structures are in blue. (For interpretation of the references to color in this figure legend, the reader is referred to the web version of this article.)

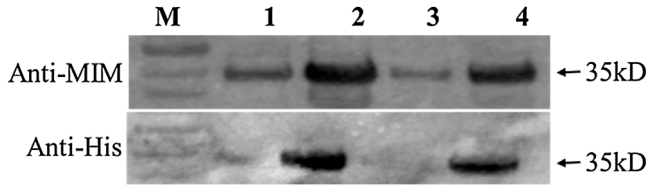

Fig. 3. Western blot image. Supernatant of lysate cells without induction (lane1 and lane 3), induced after 25 °C, 12 h (lane2) and 37 °C, 3 h (lane4).

out induction (lane1 and lane 3), induced at 25 °C for 12 h (lan2), and at 37 °C for 3 h (lane4) respectively. Stripes appeared in lane2 and lane4, indicating that His-tagged MIM-I-BAR was successfully expressed as the N-terminal histidine fusion protein in *E. coli*.

3.2. Optimization of purification process

Fig. 4A showed the SDS-PAGE images of supernatant and pellet, which reveal that MIM-I-BAR has low solubility and mainly exist in pellet as inclusion body. In order to improve the solubility, as well as to avoid the denaturation and renaturation processes, we tried four kinds of lysate method. The product was dealt with typical lysate buffer (20 mM pH 7.5 Tris/HCl, 500 mM NaCl, 10 mM imidazole, 1 mM PMSF) (Method 1), or dealt with typical lysate buffer added 0.2 mg/ mL lysozyme, 1 uL/mL protease inhibitor cock-

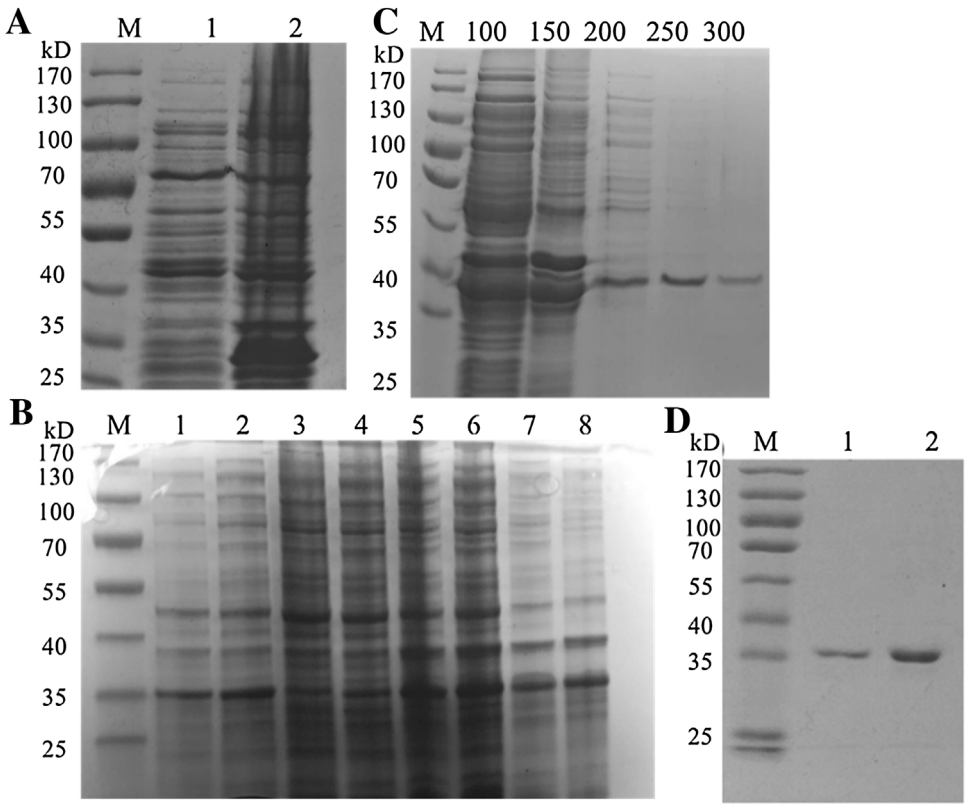

Fig. 4. 10% SDS-PAGE images. (A) Supernatant (lane1) and pellet (lane2) (B) Different kinds of lysis methods. Lane 1–4 correspond to the supernatants of lysis product after four lysate methods, and lane 5–8 correspond to the pellet of lysis product after four lysate methods. (C) Different imidazole concentrations. (D) The products without (lane1) and with (lane2) ultrafiltration.

tail (addition lysate buffer) (Method 2), or dealt with typical lysate buffer followed by being stored at −80 °C overnight (Method 3), or dealt with addition lysate buffer followed by being stored at −80 °C overnight(Method 4). The lysis products were measured by 10% SDS-PAGE and the corresponding results was shown in Fig. 4B. From Fig. 4B we may see that, at 35 kDa the gray levels of Lane 2 was higher than that of the other lanes and lane3 was lower than that of the other lanes, indicating that the treatment in the lysate buffer with protease inhibitor cocktail could obviously improve solubility of the protein in the product, in addition, overnight storage in −80 °C will decrease protein solubility. With more MIM-I-BAR dissolved in lysate buffer, the concentration of purified protein has significantly increased.

The accompanying proteins and small molecular impurities are the main factors affecting the purity and activity of the obtained MIM-I-BAR products. Here, the histidine tag was added to the N-terminus of MIM-I-BAR to facilitate the purification of the protein using a Ni-NTA agarose affinity column. Four concentrations of imidazole (100, 150, 200, and 250 mmol L^{-1}) were tested to determine the most suitable conditions for the usage of imidazole on getting rid of the accompanying proteins. According to the results of preliminary experimental (Fig. 4C), the concentration of imidazole was determined to be 200 mM or 250 mM. The eluent was then handled with PD-10 desalination column, followed by an additional ultrafiltration process to remove the small molecular impurities. Finally, the protein was separated by SDS-PAGE (Fig. 4D). The purity was determined by Quantity One (Bio-Rad) to be up to 90%.

3.3. Different purification process analyzed by AFM

As discussed above, the purity of MIM-I-BAR was dramatically improved by the purification processes in this work. However, the detailed conformation of the product after each purification process was unknown, especially the conformation of the final product. The observation of the microstructures is an effective method for the determination of the products, and is of great importance in their further applications in bioengineering. Here, the morphology of the products (after ultrafiltration) in our work was observed on mica surface by high-resolution AFM (Fig. 5). From the topography and amplitude images in Fig. 5A, we may see that the sizes of molecules under the same off-set in z direction divided into two major groups (pointed by yellow and blue arrows respectively in Fig. 5A). As we know, BAR domains are coiled-coil motifs that dimerize into modules with a positively charged surface [17]. Thus, MIM dimers is unavoidable in the final products. Fig. 5B is the zoom-in AFM image of one representative molecule from the larger-size group. From the zoom-in image and its corresponding 3-D image in Fig. 5C, we may see that these oligomers appeared to have two subunits under high-resolution AFM imaging, in accordance with the dynamics simulation results of MIM dimer in Fig. 5C. Thus, we suppose that the observed dots with larger sizes were the self-assembled MIM dimers while the smaller ones were MIM monomers. To be mentioned, the various orientations of MIM dimers on the mica surface induced the different conformations observed in Fig. 5A. All these results indicated that the obtained recombinant MIM-I-BAR protein molecules here are with high purity and remain the natural bioactivity of *in vitro* self-dimerization.

Before the ultrafiltration process, the purification went through three other processes including *E. coli* lysate, affinity chromatography, and desalination. Fig. 6A is the SDS-PAGE images of the products after *E. coli* lysis (Lane1), purified by Ni-NTA Column (Lane2), dealt with PD-10 column (Lane 3), and after ultrafiltration (Lane 4) respectively. As shown in Fig. 6A, in higher concentration, we cannot find any obvious difference among the purification steps,

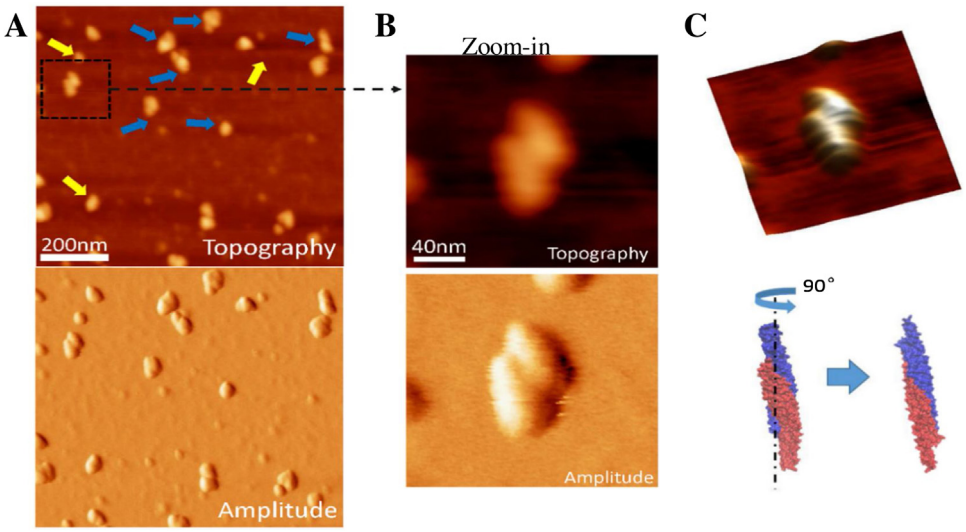

Fig. 5. (A) The topography and the corresponding amplitude AFM image of MIM-I-BAR molecules on mica surface. The ones pointed by blue arrows are supposed to be the MIM dimers, while the ones pointed by yellow arrows are supposed to be the MIM monomers. (B) The *zoom-in* AFM image of the area circled black white dashed square and its corresponding amplitude image. (C) 3D image and the molecular dynamic simulation results of MIM dimer. (For interpretation of the references to color in this figure legend, the reader is referred to the web version of this article.)

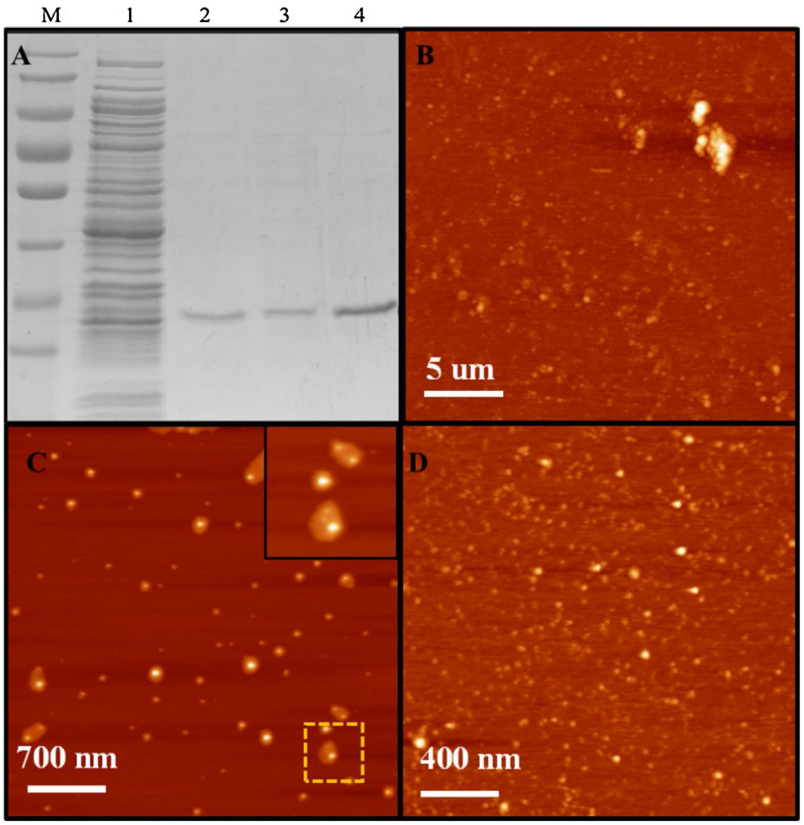

Fig. 6. (A) SDS-PAGE images of the samples after *E. coli* lysis (Lane1), purified by Ni-NTA Column (Lane2), dealt with PD-10 column (Lane 3) and after ultrafiltration (Lane 4). (B-D) The AFM imagines of the samples after *E. coli* lysis (Lane1), purified by Ni-NTA Column (Lane2), dealt with PD-10 column (Lane 3), respectively.

especially before and after desalination on the conformations of the products. And the corresponding topography AFM images of the conformations of the products after the first three were shown in Fig. 6B–D, respectively. From Fig. 6, we may see that the morphologies of the observations changed a lot for different steps. For the samples obtained after lysate process, the sizes of the observations on mica surface were varied and larger aggregations were observed (Fig. 6B). This is because that there were many impurities remaining in the products after lysate process, such as microorganism debris, other functional proteins and various salts. With the usage of Ni-NTA column to get rid of most impurities (chromatography process), the products showed more uniform distribution of size in Fig. 6C.

Interestingly, we observed fried egg-like structure in Fig. 6C. Fig. 7 is the dynamic simulation results of the MIM imidazole system and the MIM imidazole water system in the martini coarse

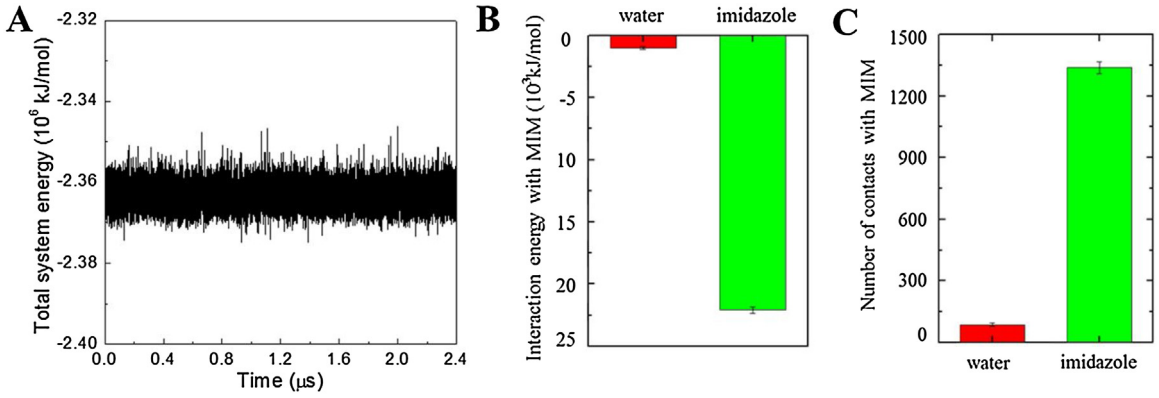

Fig. 7. (A) Time evolution of system energy, which indicates that the first 400 ns may be sufficient for the system equilibrium. (B) Non-bonded interactions between MIM I-BAR and Water/Imidazole. (C) Number of contacts between MIM I-BAR and Water/Imidazole.

grained force field, respectively. From the time evolution of the system energy shown in Fig. 7A, we may see that the system reached a balance after 400 ns. As shown in Fig. 7B, the interaction energy between MIM protein and water is much higher than that between MIM and imidazole, which indicates MIM is more likely to interact with imidazole. Besides, the number of contacts among MIM, water and imidazole is investigated in Fig. 7C. From Fig. 7C, we may see that in the mixed solution, the number of contacts between water and MIM is less than that between imidazole and MIM, indicating that the observed fried egg-like structure in Fig. 6C was attributed to the co-existence of imidazole and salts surrounding the target protein *via* nonspecific interactions (video of molecular dynamics simulation result is shown in supply information).

As reported by other publications, the small molecules surrounding the target protein effect the biological activities of the latter [18]. In order to liberate the MIM protein, we decreased the imidazole concentration *via* desalination column (Section 3.2), and the conformation of the resulted products was also investigated by AFM (Fig. 6D). As shown in Fig. 6D, the heights of the observed particles divided into two major groups under the same off-set in z direction. According to the dynamic simulation results discussed above, the less bright ones are supposed to be the previously gathered imidazole in high concentration, which dispersed into smaller fragments when the concentration of imidazole decreased. Accordingly, the brighter ones are supposed to be the liberated target protein, MIM-I-BAR. The existing smaller fragments were further removed by ultrafiltration process (Section 3.2, Fig. 4D), and we could clearly observe the target protein in forms of monomers and dimers in Fig. 5A. So far, based on the high-resolution AFM imaging, we can conclude that the desalination and ultrafiltration processes are indispensable in the purification processes of proteins to avoid to the interference of the excess salts on the morphologies and biological activities of the target protein.

4. Conclusion

By optimizing the purification process including changing the conditions of cell lysate and protein elution, we successfully purified MIM protein which is a specific protein with low solubility. The purity of the obtained protein was up to ~90%. Compared to traditional purity detection means such as SDS-PAGE, AFM provides more visual images, ensuring that we can observe the microenvironment around the target protein, as well as the conformations of the purification products following each purification process. MIM protein with two different sizes were observed on mica surface with AFM. Combining molecular dynamics simulations, these molecules were revealed as MIM monomer and dimer. Furthermore, our study attaches importance to the usage of imidazole with suitable concentrations during the affinity chromatography process, as well as the removal of excessive imidazole after the affinity chromatography process. All these results indicate that the method described here was successful in purifying MIM protein and maintaining their natural properties, and is supposed to be used to purify other proteins with low solubility.

Acknowledgement

This work was supported by the National Natural Science Foundation of China (NSFC) for Key Project of International Cooperation [grant numbers 61420106012], National Natural Science Foundation of China [grant numbers 61601227], Nature Science Foundation of Jiangsu Province [grant numbers BK20160939], Natural Science Foundation of the Jiangsu Higher Education Institutions of China [grant numbers 16KJB180010], the Fundamental Research Funds for the Central Universities and the Graduate Research and Innovation Program of Jiangsu Province in China [grant numbers KYLX15-0167], and the Collaborative Innovation Center of Suzhou Nano Science and Technology [grant numbers SX21400213].

Appendix A. Supplementary data

Supplementary data associated with this article can be found, in the online version, at http://dx.doi.org/10.1016/j.colsurfb.2017.05.054.

Video: molecular dynamics simulation result of MIM imidazole water system;

*.itp files: detailed parameters for the simulations.

References

[1] A. Frost, V.M. Unger, P.D. Camilli, The BAR domain superfamily: membrane-molding macromolecules, Cell 137 (2009) 191–196.
[2] F. Wang, Y. Liu, H. Zhang, Loss of MTSS1 expression is an independent prognostic factor for hilar cholangiocarcinoma, Pathol. Oncol. Res. 19 (2013) 815–820.
[4] L.M. Machesky, S.A. Johnston, MIM: a multifunctional scaffold protein, J. Mol. Med. 85 (2007) 569–576.
[5] G. Bompard, S.J. Sharp, G. Freiss, L.M. Machesky, Involvement of Rac in actin cytoskeleton rearrangements induced by MIM-B, J. Cell Sci. 118 (2005) 5393–5403.
[6] A. Yamagishi, M. Masuda, T. Ohki, H. Onishi, N. Mochizuki, A novel actin bundling/filopodium-forming domain conserved in insulin receptor tyrosine kinase substrate p53 and missing in metastasis protein, J. Biol. Chem. 279 (2004) 14929–14936.
[7] P.K. Mattila, A. Pykäläinen, J. Saarikangas, V.O. Paavilainen, H. Vihinen, E. Jokitalo, P. Lappalainen, Missing-in-metastasis and IRSp53 deform PI(4,5)P2-rich membranes by an inverse BAR domain-like mechanism, J. Cell Biol. 176 (2007) 953–964.

[8] S. Kunze, K. Lemke, J. Metze, G. Bloukas, K. Kotta, C.H. Panagiotidis, T. Sklaviadis, W. Bodemer, Atomic force microscopy to characterize the molecular size of prion protein, J. Microsc. 230 (2008) 224–232.
[9] Z. Lou, B. Wang, C. Guo, K. Wang, H. Zhang, B. Xu, Molecular-level insights of early-stage prion protein aggregation on mica and gold surface determined by AFM imaging and molecular simulation, Colloids Surf. B Biointerfaces 135 (2015) 371–378.
[10] S.J. Marrink, H.J. Risselada, S. Yefimov, D.P. Tieleman, A.H.D. Vries, The MARTINI force field: coarse grained model for biomolecular simulations, J. Phys. Chem. B 111 (2007) 7812–7824.
[11] M.J. Abraham, T. Murtola, R. Schulz, S. Páll, J.C. Smith, B. Hess, E. Lindahl, GROMACS: high performance molecular simulations through multi-level parallelism from laptops to supercomputers, Softwarex 1 (2015) 19–25.
[12] W. Humphrey, A. Dalke, K. Schulten, VMD: visual molecular dynamics, J. Mol. Graph. 14 (1996) 33.
[13] S.J. Marrink, H.J. Risselada, S. Yefimov, D.P. Tieleman, A.H.D. Vries, The MARTINI force field: coarse grained model for biomolecular simulations, J. Phys. Chem. B 111 (2007) 7812.
[14] G. Bussi, D. Donadio, M. Parrinello, Canonical sampling through velocity rescaling, J. Chem. Phys. 126 (2007) 014101.
[15] M. Parrinello, A. Rahman, Polymorphic transitions in single crystals: a new molecular dynamics method, J. Appl. Phys. 52 (1981) 7182–7190.
[16] S.H. Lee, F. Kerff, D. Chereau, F. Ferron, A. Klug, R. Dominguez, Structural basis for the actin-binding function of missing-in-metastasis, Structure 15 (2007) 145–155.
[17] M. Cao, Y.E. Ziqi, X.B. Lin, G.U. Ning, Advances in missing-in-metastasis research, Chin. Sci. Bull. 60 (2015) 356–366.
[18] Q. Zhang, Y. Ni, S. Kokot, Molecular spectroscopic studies on the interaction between ractopamine and bovine serum albumin, J. Pharm. Biomed. Anal. 52 (2010) 280–288.